JOURNAL OF GUIDANCE, CONTROL, AND DYNAMICS
Vol. 20, No. 4, July–August 1997

Near-Optimal Control of Altitude and Path Angle During Aerospace Plane Ascent

Jean-Paul Kremer*
Princeton University, Princeton, New Jersey 08544
and
Kenneth D. Mease†
University of California, Irvine, Irvine, California 92697

Altitude and flight-path-angle control during the posttransonic airbreathing segment of aerospace plane ascent is addressed, with objectives to minimize fuel usage and respect the vehicle flight envelope. Based on a time-scale separation between energy/mass and altitude/path-angle dynamics, the altitude/path-angle control problem is viewed in a singular perturbation framework as an initial boundary-layer problem. A feedback law approximating the minimum-fuel initial boundary-layer control is obtained by solving a neighboring-optimal problem. To facilitate this derivation, the state constraint that is active on the slow solution is modeled in the boundary layer using an appropriate penalty function. The neighboring-optimal feedback law performs well as long as temporary constraint violations are acceptable in the boundary layer. An alternate linear feedback law is derived with gains calculated to reduce constraint violations, but this law leads to increased fuel usage. Numerical results are presented for a lifting-body configuration of an aerospace plane and a Mach 8 flight condition. The results show that fuel usage and control activity are reduced when the peak dynamic pressure is allowed to increase. Differences in fuel usage are small for the vehicle model employed.

Nomenclature

E = specific energy of vehicle
f = engine fuel flow rate
H = Hamiltonian function, hard constraint formulation
$\tilde{H}$ = Hamiltonian function, soft constraint formulation
K = penalty parameter
m = mass of vehicle
P = penalty function
Q = convective heating rate at stagnation point
$\bar{q}$ = dynamic pressure, $0.5\rho V^2$
R = net aerodynamic and propulsive force
R_N = component of R normal to velocity vector and in longitudinal plane
R_T = component of R parallel to velocity vector
r = radius from Earth's center
S = state inequality constraint boundary
t = time
t_f = final time
t_0 = initial time
U = set of feasible controls
$\boldsymbol{u}$ = control vector, $(\alpha \;\; \pi^T)^T$
V = inertial velocity
$\boldsymbol{x}$ = slow state vector, $(E \;\; m)^T$
$\boldsymbol{z}$ = fast state vector, $(r \;\; \gamma)^T$
α = angle of attack
γ = inertial flight-path angle
$\delta(\,)$ = error relative to zeroth-order slow solution, $(\,)-(\,)_0^s$
ε = singular perturbation parameter
$\boldsymbol{\lambda_x}$ = slow adjoint vector, $(\lambda_E \;\; \lambda_m)^T$
$\boldsymbol{\lambda_z}$ = fast adjoint vector, $(\lambda_r \;\; \lambda_\gamma)^T$
μ_e = Earth's gravitational constant
π_k = throttle command of engine k
$\boldsymbol{\pi}$ = throttle command vector, $(\pi_1 \;\; \pi_2 \;\; \cdots)^T$
ρ = atmosphere density
υ = stretched time, $(t - t_0)/\varepsilon$

Subscripts and Superscripts

$(\,)^i$ = initial boundary-layer solution
$(\,)_{\max}$ = maximum value
$(\,)_{\min}$ = minimum value
$(\,)^s$ = slow solution
$(\,)^T$ = transpose of a matrix
$(\,)_0$ = value at t_0
$(\,)_0^i$ = zeroth-order approximation of $(\,)^i$
$(\,)_0^s$ = zeroth-order approximation of $(\,)^s$

Introduction

A SINGLE-STAGE-TO-ORBIT vehicle that uses both airbreathing and rocket propulsion to accelerate to orbital velocity is referred to here as an aerospace plane. The objective in developing an aerospace plane is to deliver payloads to low Earth orbit at a fraction of the cost of using existing rocket-powered launch vehicles. As with rocket-powered launch vehicles, an aerospace plane must ascend along a near minimum-fuel trajectory in order to maximize its payload capability. The minimum-fuel trajectory for an aerospace plane is, however, substantially different from that of a rocket-powered vehicle. Whereas a rocket-powered vehicle leaves the dense atmosphere quickly to minimize drag losses, an aerospace plane flies much longer in the dense atmosphere where the airbreathing propulsion is most efficient. The ascent guidance for an aerospace plane must steer the vehicle along the minimum-fuel trajectory and include logic for switching between rocket propulsion and the various modes of airbreathing propulsion, such as ramjet and scramjet. To minimize the fuel margin required to handle off-nominal conditions, the ascent guidance should be closed loop.

A promising ascent guidance approach capitalizes on a two-time-scale separation in the longitudinal point-mass dynamics under the fuel minimizing control program. This approach to the aerospace plane ascent guidance appears to have been proposed independently by Corban et al.,[1] Schultz et al.,[2] and Sauvageot et al.[3] The approach

Presented as Paper 94-3634 at the AIAA Guidance, Navigation, and Control Conference, Scottsdale, AZ, Aug. 1–3, 1994, and as Paper 95-3329 at the AIAA Guidance, Navigation, and Control Conference, Baltimore, MD, Aug. 7–10, 1995; received April 24, 1996; revision received March 7, 1997; accepted for publication March 10, 1997.

*Graduate Student, Department of Mechanical and Aerospace Engineering; currently Researcher, Faculte des Sciences Appliquees, Service d'Electronique, Universite Libre de Bruxelles, Avenue F.D. Roosevelt, 50, CP 165, B-1050 Brussels, Belgium. Member AIAA.

†Associate Professor, Mechanical and Aerospace Engineering. Associate Fellow AIAA.

was further developed in Refs. 4–10. The ascent guidance problem is decomposed into a slow subproblem involving the energy and mass dynamics and boundary-layer subproblems involving the faster altitude and flight-path-angle dynamics. The solution to the slow subproblem is approximated by determining, pointwise in time, the control values that maximize the energy gain per unit mass of fuel consumed.[1] Except for boundary-layer corrections, the slow solution accurately approximates the full-state minimum-fuel solution during the posttransonic airbreathing segment of the ascent (between Mach 3 and Mach 16, approximately) for conical vehicle models[5,11] and for lifting-body vehicle models.[10,12] Thus the time-scale separation seems to be a generic feature of the longitudinal point-mass dynamics under the minimum-fuel ascent control program. The general analysis by Calise et al.[13] provides further support for this conclusion. Another guidance approach for airbreathing launch vehicles, based on numerical real-time solution of the full-state optimal control problem, has been proposed by Paus and Well.[14]

Although only a partial solution to the guidance problem, the approximate slow solution has been used to characterize the minimum-fuel ascent trajectories for a variety of aerospace plane models.[1–10] These results, together with those in Refs. 11 and 12, revealed that a common characteristic of the minimum-fuel trajectories is flight at maximum dynamic pressure or maximum heating rate, whichever is most constraining, during significant segments of the ascent. By operating on the flight envelope boundary, maximum performance of the airbreathing engines is achieved.

Following the two-time-scale approach, the guidance solution is constructed by matching initial and final boundary-layer solutions to the slow solution.[15] If there is a discontinuity in the slow solution at an intermediate time, a transition layer connecting the slow solution is also needed.[9] Our attention here is on the initial boundary layer. Treating state constraints such as maximum dynamic pressure and maximum heating rate as hard constraints in the boundary layers can be problematic. Corban et al.[1] and Calise and Corban[16] noted that when the zeroth-order approximation of the minimum-fuel slow solution lies on a state constraint boundary, the zeroth-order initial boundary-layer solution may reach the slow solution in finite time on the fast time scale. Although this is interesting mathematically, it complicates obtaining the boundary-layer solution in feedback form. Moreover, for guidance, initial conditions that violate a state constraint must be considered, but they cannot be handled by the hard constraint formulation. As an alternative to the minimum-fuel, hard constraint formulation, Corban et al.[1] posed the boundary-layer guidance subproblem as that of tracking the minimum-fuel slow solution. They linearized the altitude and flight-path-angle dynamics by feedback linearization and designed a feedback control for asymptotic tracking. The feedback linearization approach was extended to constraint tracking[5] and later combined with variable structure control to obtain a robust tracking law.[6] Lu[17] proposed a similar tracking law employing feedback linearization. These tracking laws[1,5,6,17] were derived without accounting for fuel usage and flight envelope boundaries.

In this paper, we consider the initial boundary-layer guidance subproblem, in cases where the slow solution lies on a state constraint boundary. Our primary objective is to develop a method for obtaining a feedback law that approximates the minimum-fuel initial boundary-layer solution. This feedback law is to be used for altitude/path-angle control during the posttransonic airbreathing segment of the ascent. In our developments, we consider specifically the case where the slow solution is on the dynamic pressure boundary, but our approach is applicable to other state constraint boundaries, such as that for heating rate. We treat the dynamic pressure constraint as a soft constraint by adding a penalty function to the boundary-layer performance index. With a judicious choice of penalty function, it is possible to derive an approximate feedback solution to the initial boundary-layer problem. Moreover, the proposed soft constraint formulation provides solutions for initial conditions located on both sides of the constraint boundary. Treating a state constraint as soft in the initial boundary layer was previously proposed by Markopoulos and Calise,[18] although not specifically applied to flight guidance.

The solution method is evaluated using the aerospace plane model in Ref. 12. This model is for a lifting-body configuration of aerospace plane and has pronounced aeropropulsive interactions. The aerodynamic angle of attack influences the performance of the airbreathing engines. The operation of the engines affects the airflow and pressure distribution over large surfaces of the vehicle and generates a force with significant components in both the axial and normal directions. The implications of these aeropropulsive interactions for attitude and flexible structure control are analyzed in Ref. 19. Determining the effects of aeropropulsive interactions on the minimum-fuel altitude/path-angle solutions is another objective of our study.

The paper is organized as follows. The formulation of the aerospace plane minimum-fuel ascent problem, the derivation of the necessary conditions for optimality, and the two-time-scale structure of the solution are first recalled. The initial boundary-layer subproblem is then considered in detail. The initial boundary-layer subproblem is formulated for both hard and soft versions of a maximum dynamic pressure constraint. For the latter case, a family of penalty functions is constructed. A feedback approximation of the soft constraint solution is derived by solving a neighboring-optimal problem. A simpler, suboptimal feedback law is also derived. Numerical solutions of the initial boundary-layer problem are presented for the vehicle model in Ref. 12 and a Mach 8 flight condition and are evaluated and compared with the feedback solutions.

Minimum-Fuel Ascent Problem

The ascent trajectory is assumed to evolve in a great circle plane. The point-mass state of the aerospace plane is represented by its specific energy, mass, radius from Earth's center, and flight-path angle. The control variables are the aerodynamic angle of attack and the throttles of the airbreathing and rocket engines. The lateral dynamics are not considered. The Earth is assumed spherical and nonrotating, its gravity field following the inverse square law. The equations of motion are

$$\frac{\mathrm{d}E}{\mathrm{d}t} = \frac{V R_T(E, r, \gamma; \alpha, \pi)}{m} \tag{1a}$$

$$\frac{\mathrm{d}m}{\mathrm{d}t} = -f(E, r, \gamma; \alpha, \pi) \tag{1b}$$

$$\varepsilon \frac{\mathrm{d}r}{\mathrm{d}t} = V \sin\gamma \tag{1c}$$

$$\varepsilon \frac{\mathrm{d}\gamma}{\mathrm{d}t} = \frac{R_N(E, r, \gamma; \alpha, \pi)}{mV} - \left(\frac{\mu_e}{r^2} - \frac{V^2}{r}\right)\frac{\cos\gamma}{V} \tag{1d}$$

where the inertial velocity is viewed as a function of the state variables, $V = \sqrt{2(E + \mu_e/r)}^{1/2}$. The net force resulting from aerodynamics and propulsion is represented by the tangential and normal components $R_T(E, r, \gamma; \alpha, \pi)$ and $R_N(E, r, \gamma; \alpha, \pi)$. The fuel flow rate is represented by $f(E, r, \gamma; \alpha, \pi)$.

The energy-state representation is chosen because it facilitates a two-time-scale decomposition of the dynamics. The parameter ε has been introduced in Eqs. (1c) and (1d) to indicate the existence of this time-scale separation and present the equations in the standard form for applying the singular perturbation formalism. The introduction of the parameter ε in the equations of motion has sometimes been called forced singular perturbations because the actual dynamics of the vehicle correspond to $\varepsilon = 1$. State variables other than radius have been proposed for further improving the two-time-scale approximation of flight mechanics problems, mainly to improve the accuracy of the zeroth-order slow solution.[4,20,21] For initial boundary-layer control, radius and path angle are used here as fast state variables. Previous studies have validated the two-time-scale decomposition with energy and mass as slow variables and radius and flight-path angle as fast variables for the posttransonic airbreathing segment of aerospace plane ascent.[5,13]

Additional time-scale separations are assumed to exist between the point-mass dynamics and the engine dynamics, rotational pitch dynamics, fuselage structural dynamics, and unsteady

aerodynamics. The separation of the unsteady aerodynamics and engine dynamics from the point-mass dynamics is justified by the high velocity of the airflow in hypersonic flight and by the absence of high-inertia rotating machinery in the airbreathing engines. The separation of the rotational and structural dynamics from the point-mass dynamics is postulated and verified a posteriori by comparing the time scales in point-mass guidance solutions with estimates of those in closed-loop rotational and structural dynamics.

The initial conditions are

$$\boldsymbol{x}(t_0) = \boldsymbol{x}_0 = (E_0 \quad m_0)^T \tag{2a}$$

$$\boldsymbol{z}(t_0) = \boldsymbol{z}_0 = (r_0 \quad \gamma_0)^T \tag{2b}$$

From a guidance point of view, an initial condition is any reasonable flight condition during the posttransonic ascent. The guidance objective is to reach the target orbital conditions[6] while minimizing fuel consumption and respecting the flight envelope of the vehicle. The corresponding optimal control problem is posed as finding the piecewise continuous control $\boldsymbol{u}(t)$ that minimizes the performance index

$$J = -m(t_f) \tag{3}$$

subject to the differential constraints in Eqs. (1), the initial conditions in Eqs. (2), the final conditions for the target orbit, the state variable inequality constraints

$$\bar{q} \le \bar{q}_{\max} \tag{4a}$$

$$Q \le Q_{\max} \tag{4b}$$

and the control inequality constraints

$$\alpha_{\min}(\boldsymbol{x}, \boldsymbol{z}) \le \alpha \le \alpha_{\max}(\boldsymbol{x}, \boldsymbol{z}) \tag{5a}$$

$$\pi_{k\,\min}(\boldsymbol{x}, \boldsymbol{z}) \le \pi_k \le \pi_{k\,\max}(\boldsymbol{x}, \boldsymbol{z}), \qquad k = 1, 2, \ldots \tag{5b}$$

The values chosen for $\bar{q}_{\max}$ and $Q_{\max}$ in Eqs. (4) must include safety margins to avoid obtaining a solution that stresses the vehicle to its ultimate capabilities. The size of these margins affects the fuel performance achieved during nominal ascent and, as will appear later, influences the strategy for altitude/path-angle control. In the following developments, we proceed under the reasonable assumption that there is only one active state constraint at any time during the ascent, and we denote it by

$$S(\boldsymbol{x}, \boldsymbol{z}) \le 0 \tag{6}$$

We use the terms constraint boundary to designate the hypersurface where $S(\boldsymbol{x}, \boldsymbol{z}) = 0$, unconstrained region to designate the hypervolume where $S(\boldsymbol{x}, \boldsymbol{z}) < 0$, and constrained region to designate the hypervolume where $S(\boldsymbol{x}, \boldsymbol{z}) > 0$. The control inequality constraints in Eqs. (5) are subsequently denoted $\boldsymbol{u} \in U$, with U the set of admissible controls.

Necessary Conditions for Optimality

Necessary conditions for optimality for aerospace plane ascent have been obtained[1] from Pontryagin's maximum principle. They constitute a two-point boundary value problem for the state and adjoint variables $\boldsymbol{x}(t)$, $\boldsymbol{z}(t)$, $\boldsymbol{\lambda}_x(t)$, and $\boldsymbol{\lambda}_z(t)$, with additional interior point conditions at points of entry onto, or exit from, the boundary of a state constraint. The solution of the boundary value problem provides an extremal solution for the minimum-fuel ascent guidance problem. The two-time-scale structure of the minimum-fuel ascent solution can be exploited to reduce the amount of computation required to determine the solution. In this approach, an approximate solution is found by matching a slow solution with initial and final boundary-layer solutions.[15] The solution components are sought in the form of asymptotic expansions in the perturbation parameter ε. For example, the initial boundary-layer solution for the fast state $\boldsymbol{z}$ is written

$$\boldsymbol{z}^i(\upsilon, \varepsilon) = \boldsymbol{z}^i_0(\upsilon) + \varepsilon \boldsymbol{z}^i_1(\upsilon) + \varepsilon^2 \boldsymbol{z}^i_2(\upsilon) + \cdots \tag{7}$$

and similar expressions hold for $\boldsymbol{z}^s(t, \varepsilon)$, $\boldsymbol{x}^s(t, \varepsilon)$, $\boldsymbol{x}^i(\upsilon, \varepsilon)$, $\boldsymbol{\lambda}^s_x(t, \varepsilon)$, $\boldsymbol{\lambda}^i_x(\upsilon, \varepsilon)$, $\boldsymbol{\lambda}^s_z(t, \varepsilon)$, $\boldsymbol{\lambda}^i_z(\upsilon, \varepsilon)$, $\boldsymbol{u}^s(t, \varepsilon)$, and $\boldsymbol{u}^i(\upsilon, \varepsilon)$. The terms of the form $(\,)^s_0$ are usually referred to as the reduced solution. In the remaining sections of this paper, we focus our attention on obtaining the zeroth-order initial boundary-layer solution, i.e., the components $\boldsymbol{x}^i_0(\upsilon)$, $\boldsymbol{z}^i_0(\upsilon)$, $\boldsymbol{\lambda}^i_{x0}(\upsilon)$, $\boldsymbol{\lambda}^i_{z0}(\upsilon)$, and $\boldsymbol{u}^i_0(\upsilon)$.

Zeroth-Order Initial Boundary Layer

Hard Constraint Formulation

The initial boundary-layer problem is formulated[15] by changing the independent variable from t to the stretched-time variable υ. The zeroth-order initial boundary-layer equations are obtained by setting $\varepsilon = 0$, which results in the slow variables being constant,

$$\boldsymbol{x}^i_0(\upsilon) = \boldsymbol{x}^s_0(t_0) = \boldsymbol{x}_0 \tag{8a}$$

$$\boldsymbol{\lambda}^i_{x0}(\upsilon) = \boldsymbol{\lambda}^s_{x0}(t_0) \tag{8b}$$

and the fast variables obeying

$$\frac{\mathrm{d}\boldsymbol{z}^i_0}{\mathrm{d}\upsilon} = \left(\frac{\partial H}{\partial \boldsymbol{\lambda}_z}\right)^T \left(\boldsymbol{x}^i_0, \boldsymbol{z}^i_0, \boldsymbol{u}^i_0\right) \tag{9a}$$

$$\frac{\mathrm{d}\boldsymbol{\lambda}^i_{z0}}{\mathrm{d}\upsilon} = -\left(\frac{\partial H}{\partial \boldsymbol{z}}\right)^T \left(\boldsymbol{x}^i_0, \boldsymbol{z}^i_0, \boldsymbol{\lambda}^i_{x0}, \boldsymbol{\lambda}^i_{z0}, \boldsymbol{u}^i_0\right) \tag{9b}$$

The Hamiltonian function is

$$H = \lambda_E(V R_T/m) - \lambda_m f + \lambda_r V \sin\gamma + \lambda_\gamma \left\{(R_N/mV) - \left[\left(\mu_e/r^2\right) - (V^2/r)\right](\cos\gamma/V)\right\} + \nu S \tag{10}$$

where the state constraint has been directly adjoined[22] and the multiplier $\nu(\upsilon)$ satisfies

$$\nu(\upsilon) = 0, \qquad \text{when} \qquad S\left(\boldsymbol{x}^i_0(\upsilon), \boldsymbol{z}^i_0(\upsilon)\right) < 0 \tag{11a}$$

$$\nu(\upsilon) \ge 0, \qquad \text{when} \qquad S\left(\boldsymbol{x}^i_0(\upsilon), \boldsymbol{z}^i_0(\upsilon)\right) = 0 \tag{11b}$$

The control vector satisfies

$$\boldsymbol{u}^i_0(\upsilon) = \arg \max_{\bar{\boldsymbol{u}} \in U} H\left(\boldsymbol{x}^i_0, \boldsymbol{z}^i_0, \boldsymbol{\lambda}^i_{x0}, \boldsymbol{\lambda}^i_{z0}, \bar{\boldsymbol{u}}\right) \tag{12}$$

The boundary conditions for the zeroth-order initial boundary-layer problem are[15]

$$\boldsymbol{z}^i_0(0) = \boldsymbol{z}_0 \tag{13a}$$

$$\lim_{\upsilon \to +\infty} \boldsymbol{z}^i_0(\upsilon) = \boldsymbol{z}^s_0(t_0) \tag{13b}$$

At the times υ_j when the state trajectory enters or leaves the state constraint boundary, the fast adjoint variables obey the jump condition[22]

$$\boldsymbol{\lambda}^i_{z0}\left(\upsilon_j^+\right) = \boldsymbol{\lambda}^i_{z0}\left(\upsilon_j^-\right) - \frac{1}{\varepsilon}\sigma(\upsilon_j, \varepsilon)\left(\frac{\partial S}{\partial \boldsymbol{z}}\right)^T_{\upsilon_j} \tag{14}$$

where the scalars $\sigma(\upsilon_j, \varepsilon)$, $j = 1, 2, \ldots$, are nonnegative and of order ε (Ref. 16). The zeroth-order component $\boldsymbol{\lambda}^i_{x0}$ of the slow adjoint vector is continuous across the υ_j. Calise and Corban[16] have pointed out the disadvantages associated with using a hard constraint formulation in the initial boundary-layer problem, when the reduced solution at t_0 lies on a state constraint boundary. One disadvantage is that the hard constraint formulation does not provide a solution if the vehicle state is perturbed into the constrained region. This is problematic because the guidance logic must be able to respond to perturbations in arbitrary directions. A second disadvantage of the hard constraint formulation is that the derivation of a feedback approximation to the boundary-layer solution is difficult. This difficulty arises because the reduced solution at t_0, when it lies on a state constraint boundary, is in general not an equilibrium of the boundary-layer equations.[16]

Soft Constraint Formulation

Following the soft constraint (or penalty function) method, the hard state constraint is replaced with a performance index term penalizing state excursions in regions of the state space where the constraint is violated.[23,24] This is realized by augmenting the Hamiltonian with a penalty function $P(\boldsymbol{x}, z; K)$, where the parameter $K > 0$ is used here as a means of controlling the shape of the penalty function. The Hamiltonian, denoted $\tilde{H}$ to distinguish it from the Hamiltonian for a hard constraint, is

$$\tilde{H} = \lambda_E(VR_T/m) - \lambda_m f + \lambda_r V \sin\gamma + \lambda_\gamma \left\{(R_N/mV) - \left[\left(\mu_e/r^2\right) - (V^2/r)\right](\cos\gamma/V)\right\} + P \tag{15}$$

The zeroth-order initial boundary-layer equations with the soft constraint are identical to Eqs. (8), (9), and (12), with H replaced by $\tilde{H}$ everywhere, and boundary conditions are as in Eqs. (13). The adjoint variables are continuous.

The advantages gained by using a soft constraint in the initial boundary layer are that solutions exist for perturbations in arbitrary directions about the slow solution and that the sharpness of the constraint model can be adjusted by varying the parameter K. The inequality constraints in Eqs. (4) can be too conservative when searching for short duration boundary-layer solutions. Small violations of a constraint during the boundary-layer maneuvers might lead to advantageous solutions in terms of fuel consumption or other aspects of the guidance problem. A third advantage of the soft constraint formulation is that it facilitates the derivation of a feedback approximation of the boundary-layer solution, as shown in the next section.

Construction of Penalty Function

The construction of the penalty function $P(\boldsymbol{x}, z; K)$ is described for a situation where the reduced solution at t_0 lies on the dynamic pressure constraint boundary (situations along other constraint boundaries, such as the heating rate boundary, can be handled similarly). The penalty function is chosen as a two-segment polynomial in the constrained quantity, here dynamic pressure, of the form

$$P(\boldsymbol{x}, z; K) = 0 \qquad \text{when} \qquad \bar{q} < \bar{q}_{\max} - F(K) \tag{16a}$$

$$P(\boldsymbol{x}, z; K) = \frac{G(K)}{F^2(K)}\{\bar{q} - \bar{q}_{\max} + F(K)\}^2 \qquad \text{when} \qquad \bar{q} \geq \bar{q}_{\max} - F(K) \tag{16b}$$

where $\bar{q}$ is viewed as a function of the state variables, $\bar{q} = \rho(r)(E + \mu_e/r)$. The construction of the penalty function is shown in Fig. 1. By varying the value of K, the penalty function can be made mild (low K) or sharp (large K). The functions $F(K)$ and $G(K)$ are chosen such that they both decrease when K increases. Here they are chosen as

$$F(K) = \frac{2(K+1)}{K^2} \tag{17a}$$

$$G(K) = 1/K \tag{17b}$$

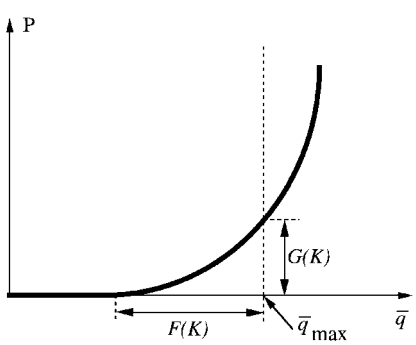

Fig. 1 Construction of penalty function for maximum dynamic pressure constraint.

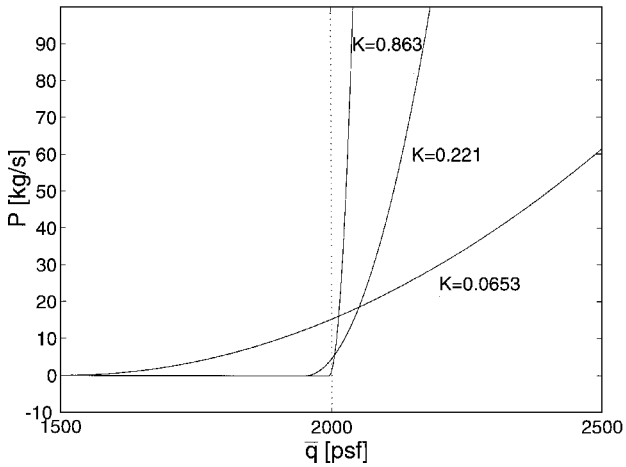

Fig. 2 Penalty functions in Eqs. (16) and (17).

Three penalty functions, corresponding to $K = 0.0653, 0.221$, and 0.863, are represented in Fig. 2 for $\bar{q}_{\max} = 2000$ psf. The choice of penalty function in Eqs. (16) and (17) will allow us to formulate a neighboring-optimal boundary-layer problem, as presented in the following section. In this regard, we point out that this penalty function and its first two derivatives with respect to $\bar{q}$ are well defined on the constraint boundary. If $\hat{\boldsymbol{x}}, \hat{z}$ denote values of the state lying on the constraint boundary, i.e., such that $\rho(\hat{r})(\hat{E} + \mu_e/\hat{r}) = \bar{q}_{\max}$, the penalty and its derivatives evaluated on the constraint boundary are

$$P(\hat{\boldsymbol{x}}, \hat{z}; K) = 1/K \tag{18a}$$

$$\frac{\partial P}{\partial \bar{q}}(\hat{\boldsymbol{x}}, \hat{z}; K) = \frac{K}{K+1} \tag{18b}$$

$$\frac{\partial^2 P}{\partial \bar{q}^2}(K) = \frac{K^3}{2(K+1)^2} \tag{18c}$$

Feedback Approximate Solutions

Determining the optimal initial boundary-layer solutions requires solving two-point boundary value problems and may not be feasible, or at least desirable, for real-time onboard guidance; determining these solutions may also not be necessary to achieve satisfactory performance. In this section, we present feedback guidance laws that require less computation and offer performance similar to the optimal initial boundary-layer solution.

The derivation of an approximate feedback solution to the initial boundary-layer problem is facilitated when the soft constraint formulation is used in the boundary layer. The reduced solution at t_0 is then an equilibrium point of the zeroth-order initial boundary-layer equations. Ardema[25] linearized the state and adjoint equations of the initial boundary-layer problem for the minimum time-to-climb problem (without state constraint) to obtain an approximate solution in feedback form. Here, with the penalty function in Eqs. (16) and (17), we are able to linearize the boundary-layer equations for state constrained problems. We derive a feedback solution by solving a neighboring-optimal problem[26] that approximates the initial boundary-layer problem. The neighboring-optimal problem consists in minimizing the second variation of the boundary-layer performance index, subject to the fast state dynamics linearized about an optimal trajectory, and to perturbed boundary conditions. The neighboring-optimal boundary-layer problem is simplest if the reduced solution at t_0 is taken as the reference optimal. It is indeed a (trivial) solution of the initial boundary-layer problem. With the error variables thus defined as

$$\delta z(\upsilon) = z(\upsilon) - z_0^s(t_0) \tag{19a}$$

$$\delta \boldsymbol{u}(\upsilon) = \boldsymbol{u}(\upsilon) - \boldsymbol{u}_0^s(t_0) \tag{19b}$$

the feedback solution takes the form

$$\delta \boldsymbol{u}(\upsilon) = -\boldsymbol{K}\delta z(\upsilon) \tag{20}$$

where the gain matrix $\boldsymbol{K}$ is obtained by solving an algebraic Riccati equation. The coefficients in the Riccati equation involve the Hessian matrix of the Hamiltonian $\tilde{H}$ with respect to z, i.e., its second derivative with respect to z, which itself involves the Hessian of the penalty function. The advantage of the penalty function defined in Eqs. (16) and (17) is that its Hessian is well defined on the constraint boundary and reflects changes in the penalty parameter K into the neighboring-optimal performance index. Also note that the state weighting matrix for this neighboring-optimal problem is indefinite, which requires special care to show the existence of a minimizing solution. This can be done following linear quadratic theory.[27] The detailed calculations for the aerospace plane application can be found in Ref. 28.

Alternatively, a simple feedback law leading to reduced constraint violations can be obtained by abandoning the neighboring-optimal formulation and employing a linear feedback of the form

$$\delta\alpha(\upsilon) = -(k_1 \quad k_2)\,\delta\boldsymbol{z}(\upsilon) \tag{21a}$$

$$\delta\pi(\upsilon) = 0 \tag{21b}$$

with the gains k_1 and k_2 calculated by a pole-placement algorithm such as to achieve a large value of the closed-loop damping coefficient. This ensures that, for initial conditions in the unconstrained region and within range of validity of the linear approximation, the closed-loop solution has a moderate overshoot into the constrained region. However, a feedback law as in Eqs. (21) is suboptimal in terms of fuel usage, as quantified in the next section.

To maintain uniform performance during the ascent, the gains for linear feedback control of altitude and path angle, whether neighboring optimal or suboptimal, must be adjusted to the slow variables energy and mass. Gain scheduling can be employed to obtain the gains in real-time onboard the vehicle. It requires only elementary onboard calculations, at the expense of data storage. Although there is no guaranteed stability and performance of the complete closed-loop system, the method should be effective, given the time-scale separation between the slow and fast translational dynamics. Ultimately, the effectiveness of gain scheduling must be verified by simulations.

Numerical Application

The performance of the optimal solutions and of the feedback approximate solutions is quantified for a Mach 8 flight condition along the posttransonic airbreathing ascent segment. The lifting-body vehicle model in Ref. 12 is used to evaluate the terms $R_T(\,)$, $R_N(\,)$, and $f(\,)$ appearing in Eqs. (1). The values of the state and control variables on the reduced solution at Mach 8 are approximated from figures of a minimum-fuel ascent trajectory in Ref. 12. The reduced solution lies on the maximum dynamic pressure boundary $\bar{q} = 2000$ psf. The airbreathing engine functions in the scramjet mode. The throttle command is the scramjet fuel flow rate. The rocket engines are not used.

Some approximations are made to simplify the calculations; however, they are not necessary. The calculations could be done without these approximations. The angle of attack is assumed small enough to have $\cos\alpha \approx 1$ and $\sin\alpha \approx \alpha$. The velocity, gravity, and Mach number are considered constant in the boundary layer (to zeroth order, the boundary layer takes place at constant energy). The aerodynamic coefficients of the vehicle and the propulsion coefficients of the airbreathing engine are approximated by polynomial expressions in the angle of attack and fuel flow rate.[28] The effects of aerodynamic control surface deflections on the aerodynamic and propulsive forces are neglected. The atmospheric density is modeled by an exponential law.

Optimal Solutions

Initial boundary-layer solutions have been calculated for different constraint models by solving the corresponding two-point boundary value problems, using a shooting algorithm. A phase portrait of the solutions in the error plane $(\delta r, \delta\gamma)$ is shown in Fig. 3. The corresponding time histories of the dynamic pressure and the controls are shown in Fig. 4. The initial conditions are $(\delta r, \delta\gamma) = (\pm 1000\,\text{ft}, 0)$. These altitude perturbations correspond to perturbations of approximately $\pm 4\%$ in atmospheric density. The

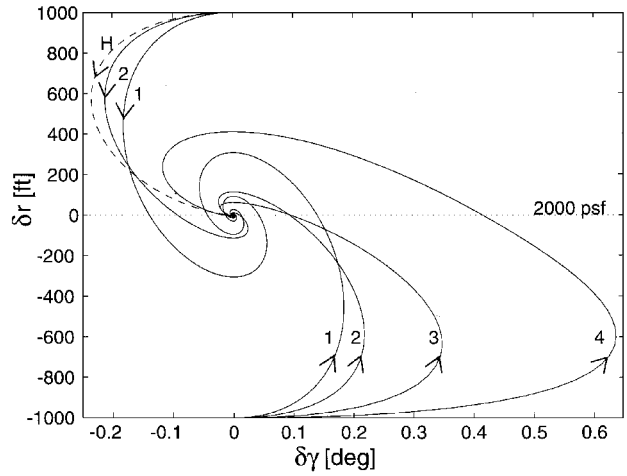

Fig. 3 Phase portraits of optimal solutions for several constraint models.

hard constraint solution is labeled H and drawn as a dashed line (note that a hard constraint solution does not exist for initial conditions in the constrained region). Soft constraint solutions are presented for four values of the penalty parameter K and are labeled 1, 2, 3, and 4. Solution 1 corresponds to a mild penalty function ($K = 0.0653$), and solutions 2, 3, and 4 are for progressively sharper penalty functions ($K = 0.221$, 0.863, and 4.83). Solutions 3 and 4 for initial condition in the unconstrained region are very close to the solution H and are sometimes omitted for clarity of the figures. The dotted line in Fig. 3 indicates the reduced solution altitude, where $\bar{q} = 2000$ psf; the region above the line is the unconstrained region where $\bar{q} < 2000$ psf, and the region below the line is the constrained region where $\bar{q} > 2000$ psf (with E constant to zeroth order, $\bar{q}$ is a function of r only).

The adjoint variable λ_h jumps at the end of the hard constraint initial boundary-layer solution to reach its reduced solution value, as predicted by Eq. (14). With the soft constraint formulation, the adjoint variables are continuous, but the hard constraint jump behavior of λ_h is approached for large values of K (Refs. 28 and 29). The soft constraint solution thus approaches the hard constraint solution as K increases.

In Ref. 29, initial boundary-layer solutions were presented for a conical configuration of aerospace plane, at Mach 6. Some qualitative differences can be observed by comparing these solutions with those presented here for a lifting-body configuration. First, the minimum-fuel throttle program is different for the two vehicle models. For the vehicle model in Ref. 12, the minimum-fuel ascent trajectory has segments flown at intermediate throttle, whereas the minimum-fuel ascent for the conical model used in Ref. 29 is flown at full throttle.[5] This difference results from the different specific impulse characteristics of the two engine models. An intermediate and varying throttle setting is required in the initial boundary layer for the vehicle model of Ref. 12, as illustrated in Fig. 4c. Another difference is that the initial boundary-layer solutions for the lifting body evolve more slowly than those for the conical vehicle and require a smaller range of variation in angle of attack. This is due partly to different flight conditions and partly to different aerodynamic and propulsive characteristics of the models. In particular, the lifting-body configuration is subject to aeropropulsive interactions, whereas the conical configuration is not.

Feedback Solutions

Trajectories for the neighboring-optimal feedback law in Eq. (20) have been simulated and compared to the optimal solutions. The neighboring-optimal solutions accurately approximate the optimal solutions when mild or medium penalty functions are used. The results with a medium penalty function are presented in Fig. 5, which shows the time histories of the dynamic pressure and the controls. A rather large initial perturbation of $(\delta r, \delta\gamma) = (+5000\,\text{ft}, 0)$ was chosen to emphasize the differences between the solutions. Figure 5 shows the hard constraint solution (dashed line), the optimal

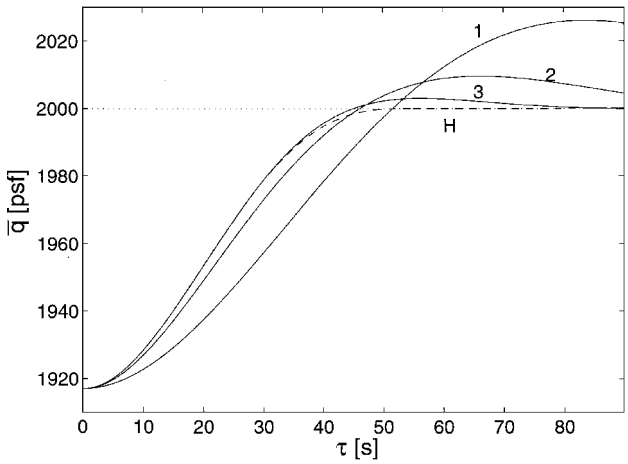

a) Dynamic pressure

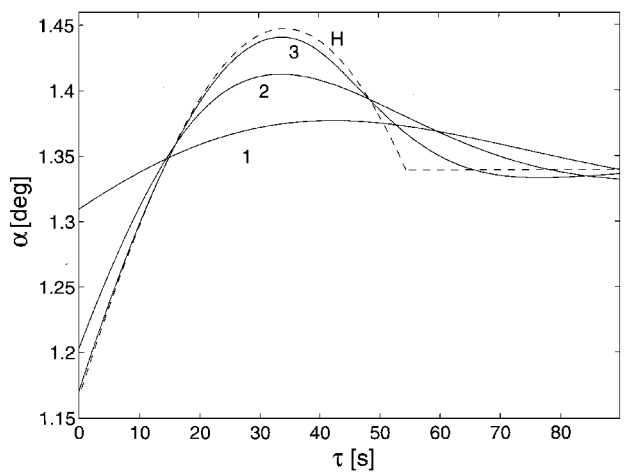

b) Angle-of-attack control

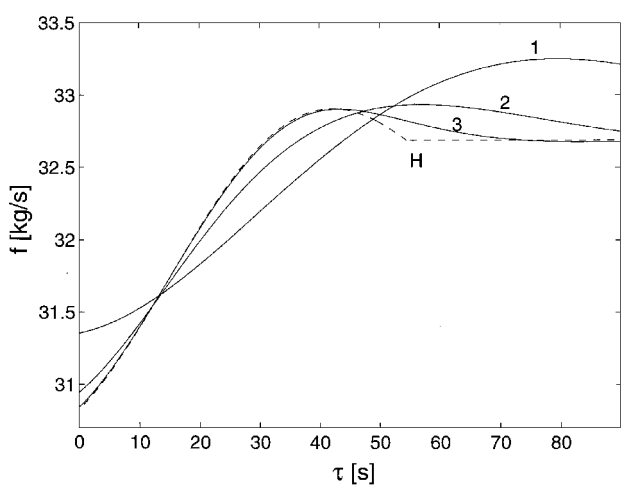

c) Scramjet fuel flow rate control

Fig. 4 Time histories of optimal solutions for several constraint models.

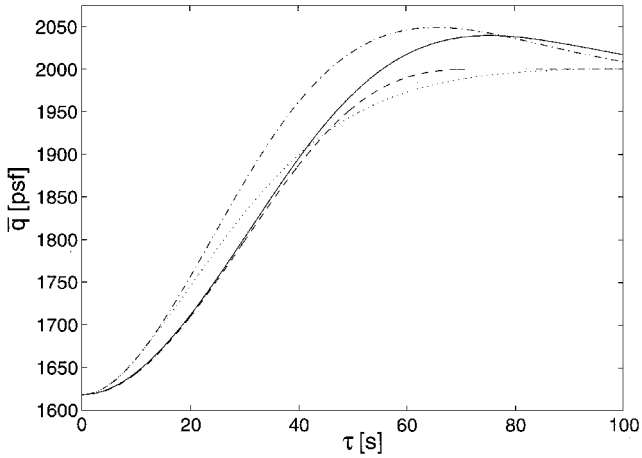

a) Dynamic pressure

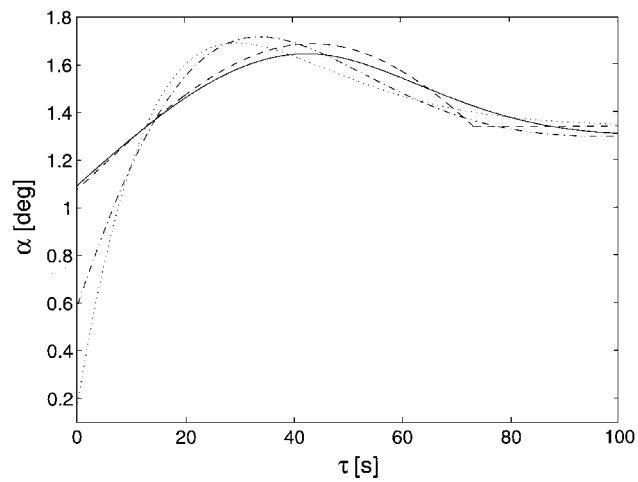

b) Angle-of-attack control

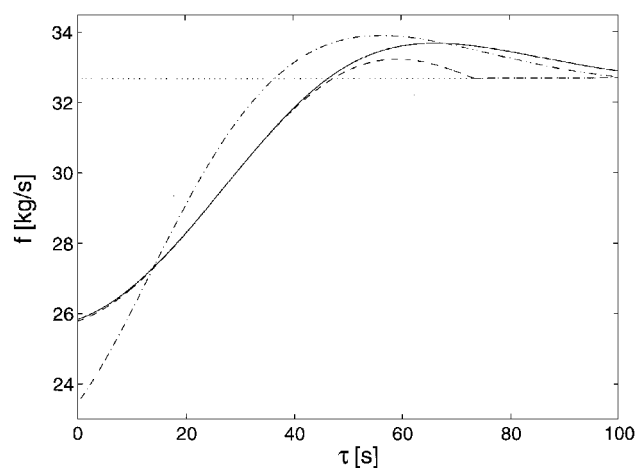

c) Scramjet fuel flow rate control

Fig. 5 Time histories of optimal, neighboring-optimal, and suboptimal solutions.

solution for a medium penalty function (solid line), the neighboring-optimal solution for the same penalty function (dash-dotted line), and the solution for the suboptimal law in Eqs. (21) (dotted line). The neighboring-optimal solution is in good agreement with the optimal solution given the large initial perturbation. For smaller perturbations, the solutions are in even better agreement. As seen in Figs. 5b and 5c, the neighboring-optimal and suboptimal solutions require more control activity than the optimal solution.

With sharp penalty functions (large K), the neighboring-optimal solutions become significantly different from the optimal solutions and are therefore unsatisfactory. This is because in the neighboring-optimal formulation a sharp state constraint introduces a large penalty on state deviations, which creates a cheap control situation. When $K \to \infty$, the closed-loop eigenvalues of the neighboring-optimal solution migrate toward infinity in the complex plane, along asymptotes disposed in a Butterworth pattern at ± 45 deg. The closed-loop frequency increases and the damping coefficient tends toward 0.707. To achieve a larger value of the damping coefficient and avoid constraint violations, a suboptimal law as in Eqs. (21) may be used instead, as illustrated in Fig. 5 (dotted line).

Evaluation of Solutions

The relative performance of the optimal, neighboring-optimal, and suboptimal boundary-layer solutions has been evaluated, for

Table 1 Comparison between altitude/path-angle solutions

	Optimal, Eqs. (9) and (12)				Neighboring optimal, Eq. (20)		
Parameter	Mild penalty	Medium penalty	Sharp penalty	Hard constraint	Mild penalty	Medium penalty	Suboptimal, Eqs. (21)
Maximum $\bar{q}$, psf	2130	2040	2009	2000	2133	2049	2001
Fuel usage, kg	3273.7	3275.4	3275.9	3276.1	3273.7	3276.1	3292.8
Time-scale separation	Poor	Good	Good	Good	Poor	Good	Good
Control activity	Good	Good	Fair	Poor	Good	Fair	Fair

different constraint models, in terms of peak dynamic pressure, fuel usage, two-time-scale separation, and control activity. The results of this comparison are summarized in Table 1. Again, an initial perturbation $(\delta r, \delta\gamma) = (+5000\,\text{ft}, 0)$ was chosen to emphasize the differences between the solutions. Fuel consumption has been measured by integrating the energy and mass dynamics during the maneuver, until a gain in specific energy $\Delta E = 1.174186\,10^{+7}\ \text{ft}^2/\text{s}^2$ was reached. This energy gain is achieved in 100 s of flight along the slow solution beginning at Mach 8, which requires 3268.9 kg of fuel. Comparing this value with the fuel consumptions in Table 1 gives a measure of the increase in fuel consumption due to the initial boundary layer.

The type of model used for the state constraint affects the two-time-scale structure of the solution. Medium and sharp penalty functions or the hard constraint are recommended to achieve sufficient time-scale separation. For control activity, the time histories in Figs. 4b and 4c show that solutions for mild or medium penalty functions generate less control activity than solutions for a sharp penalty function or the hard constraint. The magnitude and bandwidth of the excursions that must be realized in angle of attack and engine fuel flow rate may increase the demands on related vehicle systems (attitude control system, structure, engine system). In Table 1 the mild, medium, and sharp penalty functions correspond to $K = 0.0653$, 0.221, and 0.863, respectively. The gains of the suboptimal law correspond to a closed-loop period of 100 s and a damping coefficient of 0.9.

For the vehicle model employed here,[12] the fuel consumption in the initial boundary layer shows little sensitivity to changes in the penalty parameter K, whereas the extent of the dynamic pressure excursions into the constrained region changes significantly with K. Peak dynamic pressure could be maintained acceptable in the presence of constraint violations by shifting the constraint boundary in Eq. (4a). This would in turn increase the fuel consumption for a nominal ascent in unperturbed conditions. We estimate, based on the model in Ref. 12, that shifting the dynamic pressure constraint boundary from 2000 to 1900 psf (or equivalently raising the nominal altitude by about 1000 ft) would increase the fuel usage along the nominal posttransonic airbreathing segment by 0.15%, i.e., approximately 65 kg of fuel. Similarly, for a dynamic pressure constraint boundary placed at 1600 psf (altitude raised by 5000 ft), the fuel usage would increase by approximately 1% (450 kg of fuel). These numbers should be compared with the mass of payload carried by the vehicle to evaluate their significance and decide on the positioning of the constraint boundaries.

Conclusions

Based on a time-scale separation argument, the minimum-fuel altitude/path-angle control during the posttransonic airbreathing segment of an aerospace plane ascent can be approximately determined by solving, during each guidance cycle, an initial boundary-layer problem and matching its solution with a separately determined slow solution. For real-time guidance, a feedback law that at least approximates the optimal initial boundary-layer solution is preferred. A feedback law was obtained by solving a neighboring-optimal problem. For the case where the slow solution lies on a state constraint boundary, the constraint was treated in the boundary layer as a soft constraint using an appropriate penalty function. The neighboring-optimal solution performs well when a penalty function of medium sharpness is used, provided that temporary violations of the state inequality constraint are permissible.

To reduce the constraint violations, a sharp penalty function should be used; however, the performance of the neighboring-optimal feedback solution degrades with sharp penalty functions. An alternative is to use a linear feedback law with gains calculated to reduce the constraint violations. This law, however, leads to a slight increase in fuel usage.

Initial boundary-layer solutions were calculated for a lifting-body configuration of an aerospace plane and a Mach 8 flight condition. The slow solution lies on the maximum dynamic pressure constraint boundary. The boundary-layer solutions allowed us to quantify the tradeoff between limiting peak dynamic pressure on the one hand and reducing fuel usage and control activity on the other hand. Differences in fuel usage between the boundary-layer solutions are small for the vehicle/engine model employed here. Thus, the primary tradeoff is between constraint violation and control activity. Rather than incur the consequences associated with increased control activity, it may be better to bias the nominal ascent away from the true constraint boundaries of the vehicle. Our estimates indicate that the fuel increase for such biasing may be acceptable.

Acknowledgments

This research has been supported by the NASA Langley Research Center under Grant NAG1-1501 and by the Government of Luxembourg, Ministère de l'Education Nationale, under Research Scholarship BFR 94/013. The authors gratefully acknowledge this support. The authors thank an anonymous reviewer whose comments led to improvements in the paper.

References

[1] Corban, J. E., Calise, A. J., and Flandro, G. A., "Rapid Near-Optimal Aerospace Plane Trajectory Generation and Guidance," *Journal of Guidance, Control, and Dynamics*, Vol. 14, No. 6, 1991, pp. 1181–1190.

[2] Schultz, R. L., Hoffman, M. J., Case, A. M., and Sheikh, S. I., "Trajectory Optimization for Hypersonic Aircraft Guidance," AGARD-CP-504, March 1992.

[3] Sauvageot, A., Golan, O., and Breakwell, J., "Minimum Fuel Trajectory for the Aerospace-Plane," AAS/AIAA Astrodynamics Specialist Conf., Paper AAS 89-352, Aug. 1989.

[4] Moerder, D., Dutton, K., and Pamadi, B., "Constrained Variational Optimal Control Analysis of a Winged-Cone Aero-Space Plane Concept," AIAA Paper 91-5053, 1991.

[5] Van Buren, M. A., and Mease, K. D., "Aerospace Plane Guidance Using Time-Scale Decomposition and Feedback Linearization," *Journal of Guidance, Control, and Dynamics*, Vol. 15, No. 5, 1992, pp. 1166–1174.

[6] Mease, K. D., and Van Buren, M. A., "Geometric Synthesis of Aerospace Plane Ascent Guidance Logic," *Automatica*, Vol. 30, No. 12, 1994, pp. 1839–1849.

[7] Ardema, M. D., Bowles, J. V., and Whittaker, T., "Optimal Trajectories for Hypersonic Launch Vehicles," *Dynamics and Control*, Vol. 4, No. 4, Kluwer Academic, Boston, 1994, pp. 337–347.

[8] Ardema, M. D., Bowles, J. V., and Whittaker, T., "Near-Optimal Propulsion-System Operation for an Air-Breathing Launch Vehicle," *Journal of Spacecraft and Rockets*, Vol. 32, No. 6, 1995, pp. 951–956.

[9] Ardema, M. D., Bowles, J. V., Terjesen, E. J., and Whittaker, T., "Approximate Altitude Transitions for High-Speed Aircraft," *Journal of Guidance, Control, and Dynamics*, Vol. 18, No. 3, 1995, pp. 561–566.

[10] Hermann, J. A., and Schmidt, D. K., "Fuel Optimal SSTO Mission Analysis of a Generic Hypersonic Vehicle," *Proceedings of the 1995 Guidance, Navigation, and Control Conference*, AIAA, Washington, DC, 1995, pp. 1813–1823.

[11] Powell, R. W., Shaughnessy, J. D., Cruz, C. I., and Naftel, J. C., "Ascent Performance of an Air-Breathing Horizontal-Takeoff Launch Vehicle," *Journal of Guidance, Control, and Dynamics*, Vol. 14, No. 4, 1991, pp. 834–839.

[12]Chowdhry, R. S., McMinn, J. D., and Shaughnessy, J. D., "Hypersonic Vehicle Simulation Model: Lifting Body Configuration," NASA TM 109068, May 1994.

[13]Calise, A. J., Markopoulos, N., and Corban, J. E., "Nondimensional Forms for Singular Perturbation Analyses of Aircraft Energy Climbs," *Journal of Guidance, Control, and Dynamics*, Vol. 17, No. 3, 1994, pp. 584–590.

[14]Paus, M., and Well, K., "Optimal Ascent Guidance for a Hypersonic Vehicle," AIAA Paper 96-3901, July 1996.

[15]Ardema, M. D., "Singular Perturbations in Flight Mechanics," NASA TM X-62380, 2nd rev., July 1977.

[16]Calise, A. J., and Corban, J. E., "Optimal Control of Two-Time-Scale Systems with State-Variable Inequality Constraints," *Journal of Guidance, Control, and Dynamics*, Vol. 15, No. 2, 1992, pp. 468–476.

[17]Lu, P., "Inverse Dynamics Approach to Trajectory Optimization for an Aerospace Plane," *Journal of Guidance, Control, and Dynamics*, Vol. 16, No. 4, 1993, pp. 726–732.

[18]Markopoulos, N., and Calise, A. J., "Near-Optimal, Asymptotic Tracking in Control Problems Involving State-Variable Inequality Constraints," *Proceedings of the 1993 Guidance, Navigation, and Control Conference*, AIAA, Washington, DC, 1993, pp. 417–426.

[19]Chavez, F. R., and Schmidt, D. K., "Analytical Aeropropulsive/Aeroelastic Hypersonic-Vehicle Model with Dynamic Analysis," *Journal of Guidance, Control, and Dynamics*, Vol. 17, No. 6, 1994, pp. 1308–1319.

[20]Kelley, H. J., Cliff, E. M., and Weston, A. R., "Energy State Revisited," *Optimal Control Applications and Methods*, Vol. 7, No. 2, 1986, pp. 195–200.

[21]Ardema, M., and Rajan, N., "Slow and Fast State Variables for Three-Dimensional Flight Dynamics," *Journal of Guidance, Control, and Dynamics*, Vol. 8, No. 4, 1985, pp. 532–535.

[22]Jacobson, D. H., Lele, M. M., and Speyer, J. L., "New Necessary Conditions of Optimality for Control Problems with State-Variable Inequality Constraints," *Journal of Mathematical Analysis and Applications*, Vol. 35, No. 2, 1971, pp. 255–284.

[23]Kelley, H. J., "Method of Gradients," *Optimization Techniques*, edited by G. Leitmann, Academic, New York, 1962, pp. 205–254.

[24]Denham, W. F., and Bryson, A. E., Jr., "Optimal Programming Problems with Inequality Constraints. II: Solution by Steepest-Ascent," *AIAA Journal*, Vol. 2, No. 1, 1964, pp. 25–34.

[25]Ardema, M. D., "Linearization of the Boundary-Layer Equations of the Minimum Time-to-Climb Problem," *Journal of Guidance, Control, and Dynamics*, Vol. 2, No. 5, 1979, pp. 434–436.

[26]Breakwell, J. V., Speyer, J. L., and Bryson, A. E., Jr., "Optimization and Control of Nonlinear Systems Using the Second Variation," *SIAM Journal on Control*, Series A, Vol. 1, No. 2, 1963, pp. 193–223.

[27]Willems, J. C., "Least Squares Stationary Optimal Control and the Algebraic Riccati Equation," *IEEE Transactions on Automatic Control*, Vol. AC-16, No. 6, 1971, pp. 621–634.

[28]Kremer, J.-P., "Studies in Flight Guidance Involving Nonlinear Techniques and Optimization," Ph.D. Dissertation, 2041T, Dept. of Mechanical and Aerospace Engineering, Princeton Univ., Princeton, NJ, Jan. 1996.

[29]Kremer, J.-P., and Mease, K. D., "Altitude–Path Angle Control During Aerospace Plane Ascent," *Proceedings of the 1994 Guidance, Navigation, and Control Conference*, AIAA, Washington, DC, 1994, pp. 813–823.